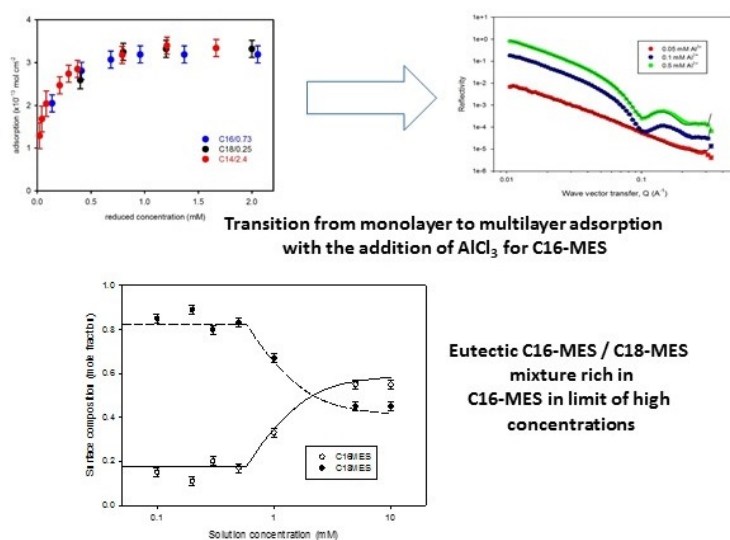


GRAPHICAL ABSTRACT

Adsorption and self-assembly in methyl ester sulfonate surfactants, their eutectic mixtures and the role of electrolyte

Hui Xu, Peixun Li, Kun Ma, Rebecca J L Welbourn, Jeffrey Penfold, Robert K Thomas, David W Roberts, Jordan T Petkov, Ken Loon Choo, Soo Yee Khoo.



Adsorption and self-assembly in methyl ester sulfonate surfactants, their eutectic mixtures and the role of electrolyte

Hui Xu¹, Peixun Li², Kun Ma², Rebecca J L Welbourn², James Douch², Jeffrey Penfold^{2,3}, Robert K Thomas³, David W Roberts⁴, Jordan T Petkov⁵, Ken Loon Choo¹, Soo Yee Khoo¹.

1. KKK Oleo, SDN BHD, Menara KKK, Muliara Damansara, 47810, Petaling, Jaya Selanger, Malaysia
2. ISIS Facility, Rutherford Appleton Laboratory, STFC, Chilton, Didcot, OXON, OX11 0QX, UK
3. Physical and Theoretical Chemistry Laboratory, Oxford University, South Parks Road, Oxford, OX1 3QZ, UK
4. School of Pharmacy and Biomolecular Sciences Liverpool John Moores University, Liverpool, L3 3AF, UK
5. Lonza UK, GB-Blackley, Manchester, Lancs, M9 8ES, UK

Corresponding author: Jeffrey Penfold, jeff.penfold@stfc.ac.uk

Keywords: Methyl ester sulfonate surfactants, adsorption at air-water interface, self-assembly, Eutectic mixture, surface multilayers, surface and micelle mixing.

ABSTRACT

The α -methyl ester sulfonate, MES, anionic surfactants are a potentially important class of sustainable surfactants for a wide range of applications. The eutectic-like Kraft point minimum in the C_{16} and C_{18} -MES mixtures is an important feature of that potential. Understanding their individual adsorption properties and the surface mixing of the eutectic mixtures are key to their wider exploitation.

Neutron reflectivity has been used to investigate the adsorption at the air-water interface of the C_{16} and C_{18} -MES surfactants and the eutectic mixture of C_{16} and C_{18} -MES, in aqueous solution and in electrolyte. The micelle mixing of the eutectic mixture is investigated using small angle neutron scattering.

The adsorption isotherms for C_{14} to C_{18} -MES are found to scale with their critical micelle concentration value. The surface and micelle compositions of the C_{16} and C_{18} -MES eutectic mixture differ from the eutectic composition; with compositions in the limit of high concentrations richer in C_{16} -MES. The mixing properties are described by the pseudo phase approximation with a repulsive interaction between the two surfactants. The impact of the multivalent ions Al^{3+} on the adsorption at the air-water interface results in a transition from monolayer to multilayer adsorption.

INTRODUCTION

The major surface active ingredients in most household detergents are anionic surfactants (1, 2). The increasing demand for improved formulations to provide better detergency, enhanced performance at lower temperatures and greater tolerance to hard water has resulted in the development of a range of new anionic surfactant structures and the optimisation of anionic / non-ionic surfactant mixtures (1-4). The alkyl sulfates, especially for the longer alkyl chain lengths, precipitate readily due to the strong binding and complexation with the multivalent ions in hard water (5-7); a common problem in limiting hard water tolerance. This can be partially mitigated by co-adsorption and self-assembly with a non-ionic co-surfactant (7). The development of the alkyl benzene sulfonate, LAS, (2, 8), and the alkyl ethoxy ether sulfate, SLES, (9-11) surfactants has greatly improved hard water detergency properties. LAS has for example demonstrated both improved detergency properties and biodegradability (1, 2).

To meet the sustainability agendas of the major detergent manufacturers there is a greater drive towards the use of surfactants prepared from renewable sustainable sources, instead of petroleum based materials (12), for greater biocompatibility and biodegradability, and for efficient operation at lower temperatures. The α -methyl ester sulfonates, MES, anionic surfactants, prepared from renewable palm-oil based sources, have been promoted as attractive alternatives to the petroleum based counterparts (13-17). Improved hard water tolerance, greater biodegradability and better cold water detergency have been demonstrated (18-22). Hence the synthesis and purification of MES has been extensively studied and reported (15, 16, 23), and the basic physicochemical properties, surface adsorption and self-assembly have been studied (23-26).

Xu et al (27) have recently reported the adsorption properties of C₁₄-MES at the air-water interface; evaluated by surface tension, ST, and neutron reflectivity, NR, and using a synthetic route to provide better defined samples. This resulted in an adsorption isotherm and limiting adsorption amounts freer from the impact of impurities, but consistent with surface divalent counterion impurities. Xu et al (28) have reported the impact of electrolyte on C₁₄-MES adsorption at the air-water interface. In NaCl, CaCl₂ and low concentrations of AlCl₃ slightly enhanced adsorption is observed, but at higher AlCl₃ concentrations surface multilayer formation occurs, ranging from a single bilayer beneath the initial monolayer at the surface to multiple bilayers. This is consistent with the more extensive studies of surface multilayer

formation with the addition of multivalent counterions with LAS and SLES at low surfactant concentrations and outside the regime of precipitation (29-32). This was demonstrated with the addition of Ca^{2+} for LAS and Al^{3+} for SLES, in which the evolution of the extent of the surface multilayers is controlled by surfactant, and counterion concentration, and the surfactant structure. The surface multilayer formation results in persistent wetting of hydrophobic solid surfaces, substantially enhanced adsorption at interfaces, and the opportunity to deliver and provide an effective surface reservoir for other surface ingredients, such as perfumes (33).

The MES surfactants can exist with a range of alkyl chain lengths, typically from C_{12} to C_{18} . Xu et al (27, 28) have focussed on the characterisation of the C_{14} -MES at the air-water interface. In this paper the focus is on the adsorption of the C_{16} and C_{18} -MES surfactants, and their eutectic mixture. One of the issues associated with the longer alkyl chain lengths is their relatively high Krafft temperatures, 28 and 40 °C for C_{16} -MES and C_{18} -MES respectively; which would suggest that the pure MES solutions would not be very effective detergents, especially at lower temperatures (18, 34). However the Krafft temperature of the C_{16} / C_{18} -MES mixture goes through a minimum at a temperature $\sim 15^\circ\text{C}$ at a composition of 65/35 mole ratio C_{16} / C_{18} -MES (35), and this mixture exhibits good detergency properties. A minimum in the Krafft point was reported in other anionic surfactant mixtures, in sodium dodecyl sulfate / bivalent metal dodecyl sulfate mixtures (36), in the sodium and calcium salts of other anionic surfactants such as the linear alkyl benzene sulfonates (37), in different alkyl benzene sulfonate mixtures (38, 39), and in myristic /palmitic acid mixtures (40); and has been likened to a eutectic point.

However little is known about the adsorption and self-assembly of such eutectic mixtures. In light of their potential importance in a range of applications the focus of this paper is on the adsorption of the eutectic mixture of C_{16} / C_{18} -MES, the individual component surfactants, and the impact of electrolyte on the adsorption, using primarily neutron reflectivity, NR. Furthermore small angle neutron scattering, SANS, is used to characterise the self-assembly of the C_{16} / C_{18} -MES eutectic mixture to primarily determine the micelle composition. The NR and SANS data are analysed and evaluated using the Pseudo phase approximation, PPA, to model the eutectic mixing behaviour. The combination of the surface and micelle compositions provides a more rigorous examination of the thermodynamics of the mixing in such systems.

EXPERIMENTAL DETAILS

The neutron reflectivity, $R(Q)$, was measured as a function of the wave vector transfer, Q , perpendicular to the surface (where Q is defined as $Q=(4\pi\sin\theta)/\lambda$, θ is the grazing angle of incidence, and λ the neutron wavelength). The measurements were made on the INTER reflectometer (41) at the ISIS pulsed neutron source in the UK; where the measurements were made at a fixed θ of 2.3° and a λ range of 1 to 15 Å to cover a Q range of ~ 0.03 to 0.3 Å^{-1} . The reflectivity was converted to an absolute scale by normalisation to the incident beam intensity and the reflectivity of a D_2O surface. The measurements were mostly made in null reflecting water, nrw, (8.8 mole % D_2O / 91.2 mole % H_2O , with a scattering length density, ρ , of 0.0, matched to air), and using deuterium labelled or a combination of deuterium labelled and unlabelled surfactants. The measurements were made in sealed Teflon troughs, with sample volumes $\sim 25 \text{ mL}$. The NR measurements for C_{16} -MES and C_{18} -MES were made at 30°C and 40°C respectively, and at 25°C for the eutectic 65/35 mole ratio C_{16} - / C_{18} -MES mixture. Each measurement took ~ 20 to 30 mins; measured sequentially on a 7 position sample changer, and repeated ~ 2 -3 times (for a total lapse time of up to 3 to 6 hours) until the reflectivity profile reached a steady state.

In the kinematic approximation (42) the neutron reflectivity is related to the square of the Fourier Transform of the scattering length density distribution, $\rho(z)$, normal to the surface; where $\rho(z) = \sum_i b_i n_i(z)$, $n_i(z)$ is the number density distribution of species i and b_i is the scattering length (the $\sum b$ values of the different components studied are listed in table 1). As the neutron scattering lengths of H and D are quite different (-3.75×10^{-5} and $6.67 \times 10^{-5} \text{ Å}$ respectively) $\rho(z)$ can be manipulated for organic species by D/H isotopic substitution. Hence deuterium labelling enables the reflectivity from different components at the interface to be isolated. This is the basis of the measurements here, as the reflectivity from a deuterium labelled surfactant adsorbed at a null reflecting air-water interface provides a direct estimate of the adsorbed amount (42). For monolayer surfactant adsorption the reflectivity is adequately modelled as a single layer of uniform composition using the exact expression for a thin film at the interface (42) to obtain a thickness, d , and scattering length density, ρ . The adsorbed amount is directly related to the $d \cdot \rho$ product such that the area/molecule, A ,

$$A = \sum b / d\rho \quad (1)$$

and the adsorbed amount $\Gamma = 1/AN_a$, and N_a is Avogadro's number. For a binary mixture of surfactants,

$$d\rho = \sum b_1/A_1 + \sum b_2/A_2 \quad (2)$$

where the subscripts 1, 2 refer to the two surfactant components. By making measurements with each component in turn deuterium labelled, A_1 and A_2 are readily determined (42). For more complex surface structures the reflectivity is usually modelled using a discrete number of layers, using the optical matrix methods (42). In modelling the NR data a flat background, typically ~ 6 to 8×10^{-6} , arising from the bulk scattering from the aqueous sub-phase, is included.

The SANS measurements were made on the LOQ diffractometer (43) at the ISIS pulsed neutron source. The measurements were made using the white beam time of flight method to cover a scattering vector, Q , range (where for SANS Q is defined as $Q=4\pi \sin(\theta/2) / \lambda$, and θ is the scattering angle) ~ 0.008 to 0.25 \AA^{-1} . The measurements were all made in 2mm path length quartz spectrophotometer cells held at 25°C . The samples were all made in D_2O , using unlabelled surfactants and a combination of labelled and unlabelled surfactants for the C_{16} - / C_{18} -MES mixture. The data were corrected for background scattering, detector response, incident spectral distribution and converted to an absolute scattered intensity, $I(Q)$, in cm^{-1} , using standard procedures (44). The SANS data is modelled assuming globular or elongated micelle structures, where the scattered intensity for interacting globular polydisperse micelles is written in the ‘decoupling approximation’ (45) as,

$$I(Q) = n \left[S(Q) \left| \langle F(Q) \rangle_Q \right|^2 + \langle |F(Q)|^2 \rangle_Q - \left| \langle F(Q) \rangle_Q \right|^2 \right] \quad (3)$$

where the averages denoted by $\langle Q \rangle$ are averages over particles size and orientation, n is the micelle number density, $S(Q)$ the structure factor, and $F(Q)$ the form factor. The micelle structure (form factor) is modelled using a standard “core and shell” model (45), as described in detail later. The inter-particle interactions are evaluated using the RMSA calculation for a repulsive screened coulombic potential between the micelle (46).

The adsorption isotherm measurements were made for C_{16} -MES and C_{18} -MES using deuterium labelled surfactants in nrw, in the MES concentration range of 0.1 to 10 mM. The adsorption of the C_{16} / C_{18} -MES eutectic mixture (65/35 mole ratio) was measured in the concentration range 0.1 to 10 mM at the fixed solution composition, using the measurements d- C_{16} -MES / d- C_{18} -MES, dd, d- C_{16} -MES / h- C_{18} -MES, dh, and h- C_{16} -MES / d- C_{18} -MES, hd, in nrw. NR measurements were also made for 0.8 mM C_{16} -MES (deuterium labelled surfactant in nrw) and AlCl_3 concentrations from 0.05 to 0.5 mM, and for 0.2 mM C_{18} -MES (deuterium labelled

surfactant in nrw) and AlCl_3 from 0.05 to 0.5 mM. Further measurements were made for the $\text{C}_{16}\text{-MES} / \text{C}_{18}\text{-MES}$ eutectic mixture (65/35 mole ratio $\text{C}_{16} / \text{C}_{18}\text{-MES}$) at a solution concentration of 0.25 mM and AlCl_3 concentrations from 0.02 to 2 mM (for d- $\text{C}_{16}\text{-MES} / \text{d-C}_{18}\text{-MES}$, dd). At 0.25 mM surfactant concentration and 0.3 mM AlCl_3 the measurements were made for the isotopic combinations dh, hd, and dd in nrw. The SANS measurements were made for the eutectic $\text{C}_{16}\text{-MES} / \text{C}_{18}\text{-MES}$ mixture (65/35 mole ratio) at concentrations of 5, 10, and 20 mM, and for the isotopic combinations hh, hd, and dh in D_2O .

Deuterium oxide, D_2O , was obtained from Sigma Aldrich, and high purity water (resistivity 18.2 MCcm) was used throughout. Analytical grade (>99.9% purity) AlCl_3 , NaCl and CaCl_2 were used as supplied by Sigma Aldrich. All the glassware, Teflon troughs, spectrophotometer cells used for the NR and SANS measurements and sample preparation were cleaned in alkali detergent (Decon90) and extensively rinsed in ultrapure water. The sodium alkyl 2-sulfo 1-methyl ester, MES, surfactants with the general formula $\text{CH}_3 (\text{CH}_2)_n \text{CH} (\text{SO}_4\text{Na}) \text{COOCH}_3$ (see figure 1), where $n=11, 13$, and 15 for $\text{C}_{14}\text{-MES}$, $\text{C}_{16}\text{-MES}$ and $\text{C}_{18}\text{-MES}$ respectively.

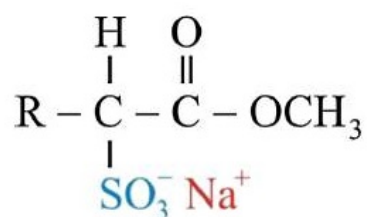


Figure 1. Structure of MES surfactant, the group labelled R is $\text{CH}_3 (\text{CH}_2)_n$.

The MES surfactants were synthesised in two forms, with and without the alkyl chain deuterium labelled and are referred to as h- $\text{C}_{14}\text{-MES}$ and d- $\text{C}_{14}\text{-MES}$ etc. The synthesis and purification are described in detail elsewhere (27).

RESULTS and DISCUSSION

(i) Adsorption Isotherms

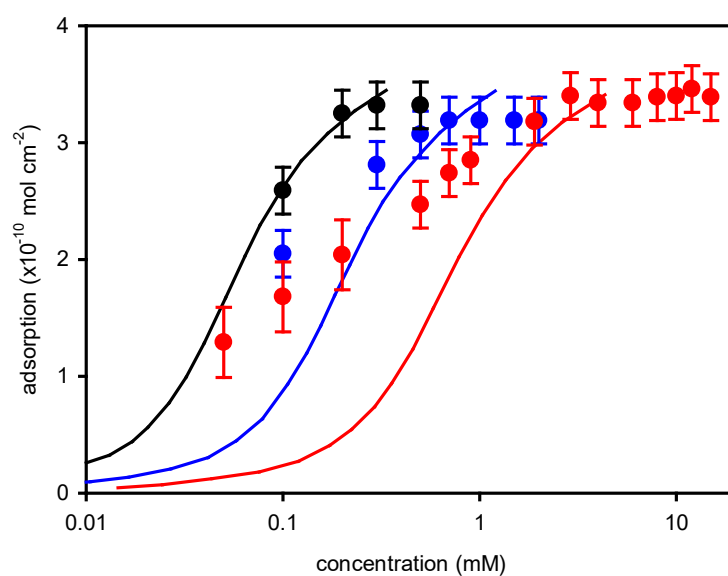
The neutron reflectivity data for d- C_{16}MES and d- C_{18}MES in nrw are well described as a thin monolayer of uniform composition, and can be modelled to obtain a thickness, d , and a

scattering length density, ρ . Over the concentration range measured the mean thickness is 19 ± 2 Å for C₁₆-MES and 20 ± 2 Å for C₁₈-MES. From the Σb values in table 1 the adsorbed amounts are obtained using equation 1.

Table 1. Σb values for different components in study (used to evaluate adsorbed amounts)

Component	Σb ($\times 10^{-3}$ Å)
d-C ₁₆ MES	3.37
h-C ₁₆ MES	0.25
d-C ₁₈ MES	3.77
h-C ₁₈ MES	0.23
nrw	0.0

In figure 2a the adsorption isotherms for C₁₆-MES and C₁₈-MES are plotted (see table S1 in the Supporting Information for the corresponding data data), along with the data for C₁₄-MES reproduced from a previous study (27). The solid lines in figure 2a are calculated isotherms reproduced from Danov et al (26). The differences between the directly measured isotherm for C₁₄-MES and that derived by Danov et al (26) were discussed recently by Xu et al (27) and were attributed to a reevaluation of the cmc determined by Danov et al (26). The discrepancies in figure 2a are progressively less pronounced as the chain length increases from C₁₄ to C₁₈, and results from a closer agreement between the actual and derived cmc values from Danov et al (26) as the alkyl chain length increases. In figure 2b the adsorption data are plotted on a reduced concentration scale, where the concentration is scaled by the surfactant cmc. Within the error of the measurements the saturation adsorption values are constant and invariant with alkyl chain length, and the isotherms overlap. This is consistent with the cmc and relative surface activity depending on the alkyl chain length. However invariance in the saturation or limiting adsorbed amount with alkyl chain length implies that the saturation adsorption is determined by the alkyl chain packing and that the headgroup plays a more secondary role. This is similar to what was reported for the SLES molecules by Xu et al (32) and for the sodium alkyl sulfates, SAS, surfactants by Varga et al (47).



(a)

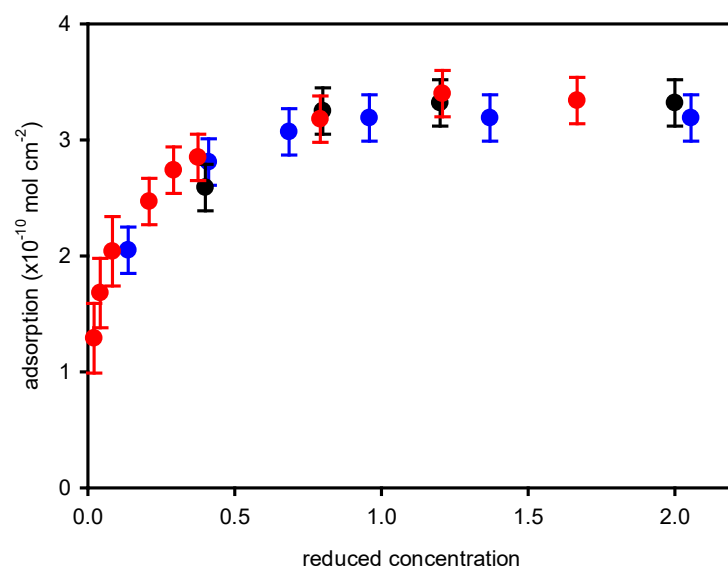


Figure 2. (a) Adsorption isotherms for C_{14} , C_{16} and C_{18} -MES measured by neutron reflectivity (data for C_{14} -MES reproduced from reference 27); the solid lines are derived isotherms from reference 26, (red) C_{14} -MES, (blue) C_{16} -MES, and (black) C_{18} -MES (b) Adsorption isotherms for C_{14} , C_{16} and C_{18} -MES plotted on a reduced concentration scale (scaled to cmc values in legend); see legend for more details.

(ii) Impact of Al^{3+} on the adsorption of C_{16} -MES and C_{18} -MES

The impact of AlCl_3 on the adsorption of C_{14} -MES has been extensively studied and previously reported (28). Here those measurements are extended to C_{16} and C_{18} -MES, and figure 3 shows the evolution of the neutron reflectivity for 0.8 mM C_{16} -MES in the presence of AlCl_3 .

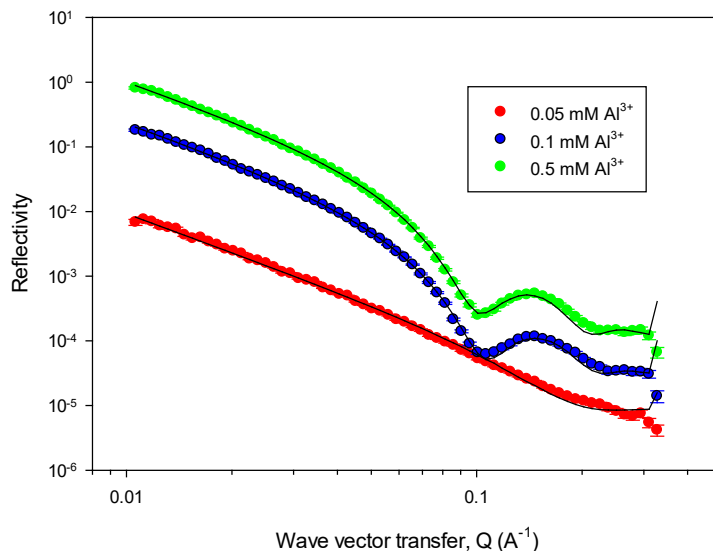


Figure 3. Neutron reflectivity for 0.8 mM C_{16} -MES in 0.05, 0.1 and 0.5 mM AlCl_3 (see legend for details). The solid lines are model calculations using the parameters in table 2 in the Supporting Information. The data for 0.1 and 0.5 mM AlCl_3 are shifted vertically by $\times 4$ and $\times 16$ respectively for clarity. See legend for more details.

At the lowest AlCl_3 concentration, 0.05 mM, the addition of AlCl_3 results in an enhanced monolayer adsorption for C_{16} -MES. At a surfactant concentration of 0.8 mM the adsorbed amount increases from $\sim 3.2 \times 10^{-10} \text{ mol cm}^{-2}$ to $\sim 3.8 \times 10^{-10} \text{ mol cm}^{-2}$, broadly comparable to the increase observed for C_{14} -MES (28). At the higher AlCl_3 concentrations, 0.1 and 0.5 mM, the pattern of adsorption is more complex and the neutron reflectivity is dominated by a broad interference fringe at relatively higher Q values. The data for 0.1 and 0.5 mM AlCl_3 are well described by a 3-layer model (see table 2 for the key model parameters) with a similar structure to give mean thicknesses for the three layers of 21, 6, $27 \pm 2 \text{ \AA}$ respectively. The 3-layer model is consistent with an initial surface monolayer and a single bilayer beneath the monolayer. The structure is similar to that reported for SLES (30-32) and more recently for C_{14} -MES (28).

Table 2. Key model parameters for fits to NR data in figure 3, for 0.8 mM C₁₆-MES in nrw, 0.05, 0.1 and 0.5 mM AlCl₃.

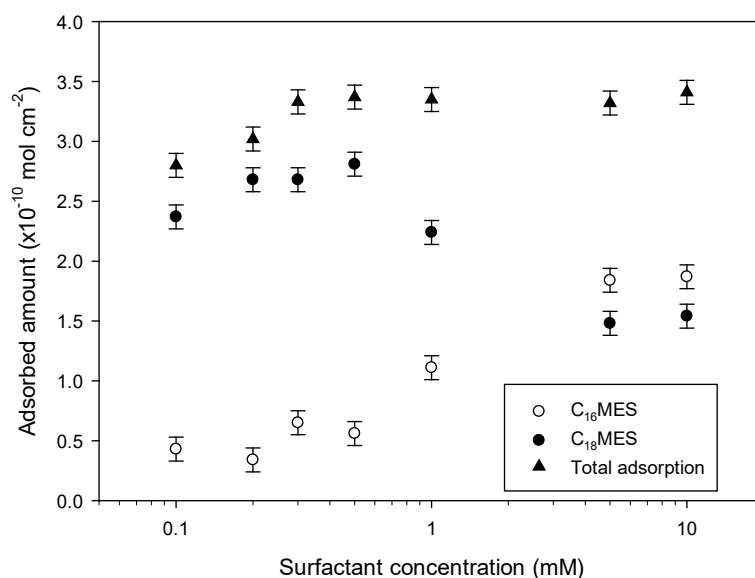
AlCl ₃ concentration (mM)	d ₁ (±1 Å)	ρ ₁ (±0.05x10 ⁻⁶ Å ⁻²)	d ₂ (±1 Å)	ρ ₂ (±0.05x10 ⁻⁶ Å ⁻²)	d ₃ (±1 Å)	ρ ₃ (±0.05x10 ⁻⁶ Å ⁻²)
0.05	26	3.10	-	-	-	-
0.10	18	3.40	6.0	1.20	33	4.00
0.50	25	3.40	7.0	0.90	21	5.60

d, ρ are the thickness and scattering length density of the layers used to model the NR data

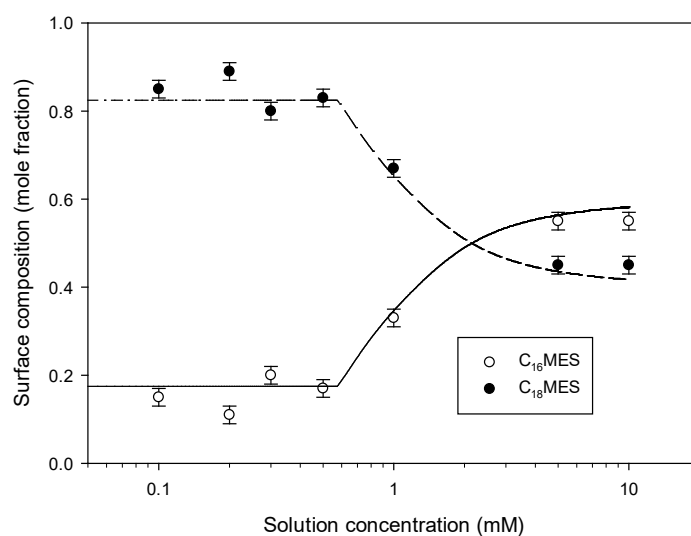
The addition of AlCl₃ to 0.2 mM C₁₈-MES in the same AlCl₃ concentration range resulted in precipitation, and the corresponding neutron reflectivity data were not consequently analysed quantitatively.

(iii) Adsorption of C₁₆-MES / C₁₈-MES mixture

As described in the Introduction a 65/35 mole ratio mixture of C₁₆-MES / C₁₈-MES shows a eutectic-like behaviour which is manifested as a pronounced minimum in the Krafft temperature. Here the surface adsorption of that eutectic binary mixture has been measured by neutron reflectivity in the solution concentration range of 0.1 to 10 mM. From neutron reflectivity measurements of the isotopic combinations d-C₁₆MES / d-C₁₈MES, h-C₁₆MES / d-C₁₈MES and d-C₁₆MES / h-C₁₈MES in nrw the total adsorption and relative amounts of C₁₆-MES and C₁₈-MES at the surface have been evaluated. The neutron reflectivity data for each isotopic combination are modelled as a single layer of uniform composition to give the product d.p. Using equation 2 for the binary mixture, and the $\sum b$ values in table 1, the 3 resulting simultaneous equations were solved using a simplex algorithm designed to solve a set of overdetermined linear equations (48). Figure 4a shows the evolution in the total adsorption and the relative amounts of C₁₆-MES and C₁₈-MES at the interface with surfactant concentration for the 65/35 mole% C₁₆-MES / C₁₈-MES mixture; and the key parameters and data are summarised in table 3.



(a)



(b)

Figure 4. (a) Variation in adsorption with surfactant concentration for 65/35 mole ratio mixture of C_{16} -MES / C_{18} -MES, (see legend for details), (b) Variation in surface composition (mole fraction) with solution concentration (see legend for details). The solid and dashed lines are model calculations using the pseudo phase approximation, as described later in the discussion.

Table 3. Adsorption data for 0.65 / 0.35 mole ratio C₁₆/C₁₈-MES mixtures, from figure 4.

Surfactant concentration (mM)	C ₁₆ -MES		C ₁₈ -MES		Total adsorption, Γ (±0.05x10 ⁻¹⁰ mol cm ⁻²)	Mole fraction C ₁₆ -MES (±0.02)
	A (Å ²)	Γ (±0.05x10 ⁻¹⁰ mol cm ⁻²)	A (Å ²)	Γ (±0.05x10 ⁻¹⁰ mol cm ⁻²)		
0.1	309±20	0.43	70±4	2.37	2.80	0.15
0.2	482	0.34	63	2.65	3.02	0.11
0.3	254±15	0.65	62	2.68	3.33	0.20
0.5	295	0.56	59	2.82	3.37	0.17
1.0	150±8	1.11	74	2.24	3.35	0.33
5.0	91±5	1.84	112	1.48	3.32	0.55
10.0	89	1.87	106	1.54	3.41	0.55

A and *Γ* are the area / molecule and adsorbed amounts as defined by equations 1 and 2.

The measurements were made over the concentration range of 0.1 to 10 mM, from below to well above the mixed cmc value. The cmc values for C₁₆-MES and C₁₈-MES are 0.75 and 0.25 mM respectively. Assuming ideal mixing the mixed cmc, C_m, can be evaluated from (49),

$$\frac{1}{C_m} = \alpha \frac{1}{C_1} + (1-\alpha) \frac{1}{C_2} \quad (4)$$

where C_m is the mixed cmc, C₁ and C₂ the cmc's of the pure components and α is the mole fraction of component 1 in solution. This gives a mixed cmc for the 65/35 mole ratio C₁₆-MES / C₁₈-MES mixture ~ 0.44 mM. For a positive β value of 1.4 used in the Pseudo phase approximation analysis (see later) the mixed cmc is 0.6 mM.

Below the mixed cmc the adsorption is dominated by the C₁₈-MES adsorption, the more surface active component. The total adsorption increases with increasing surfactant concentration up to the cmc, and around and above the cmc it is relatively constant and consistent with the individual adsorption of C₁₆-MES and C₁₈-MES (see table S1). Up to the cmc the surface composition is relatively constant with an average surface mole fraction of C₁₈-MES ~ 0.8, compared to a solution composition of 0.35. At and above the cmc the surface composition

evolves more rapidly towards a composition approaching the solution composition. However it is notable that even at ~ 20 times the cmc the surface composition is ~ 0.55 C₁₆-MES compared to a solution composition of 0.65. From a surfactant concentration ~ 5 mM and greater the surface composition hardly changes over the limited range studied and appears to be tending towards a constant value, as observed in other mixed systems (50, 51). The results also show very clearly the impact of micellisation upon the evolution in the adsorption and in the surface composition; and this is broadly similar to the trends reported by Penfold et al (50) for the non-ionic surfactant mixtures of C₁₂E₃ / C₁₂E₈ at the air-water interface. Later in the discussion a detailed evaluation of the data in the context of the pseudo phase approximation is made and discussed.

The impact of AlCl₃ on the adsorption properties of the 65/35 mole ratio eutectic mixture of C₁₆-MES / C₁₈-MES was also investigated by neutron reflectivity. Measurements were made at a fixed concentration of 0.25 mM, and AlCl₃ concentrations from 0.02 to 1.0 mM. The addition of AlCl₃ sufficiently lowers the mixed cmc such that the measurements at 0.25 mM are above the cmc (the mixed cmc is 0.6 mM in the absence of AlCl₃). At the lower AlCl₃ concentration, 0.02 mM, the adsorption is in the form of a monolayer, and at AlCl₃ concentrations > 0.02 mM the reflectivity data are dominated by a single interference fringe at relatively high Q, similar to that shown in figure 3. The nature of the reflectivity is relatively constant over the AlCl₃ concentration range from 0.05 to 1.0 mM. At an AlCl₃ concentration of 0.3 mM the measurements were made at 3 different contrasts, d-C₁₆MES / d-C₁₈dMES, h-C₁₆MES / d-C₁₈MES, and d-C₁₆MES / h-C₁₈MES in nrw. The data are shown in figure 5, and the solid lines are model calculations for the 3 layer model described earlier, and representing an initial monolayer with a single bilayer beneath it.

Table 4. Model parameters for fits to NR data in figure 5 for 0.25 mM 65/35 mole ratio C₁₆-MES / C₁₈-MES in 0.3 mM AlCl₃.

Contrast combination	$\rho_1 (\pm 0.05 \times 10^{-6} \text{ \AA}^{-2})$	$\rho_2 (\pm 0.05 \times 10^{-6} \text{ \AA}^{-2})$	$\rho_3 (\pm 0.05 \times 10^{-6} \text{ \AA}^{-2})$
dd/nrw	3.5	1.3	4.3
hd/nrw	1.9	1.5	1.5
dh/nrw	2.4	2.9	1.3
hh/D ₂ O	2.8	3.6	6.2

The layer thicknesses, d_1 , d_2 and d_3 , are constrained to 20.0, 6.0 and 33.0 respectively for all the contrasts, and ρ_1 , ρ_2 , ρ_3 are scattering length densities of the layers.

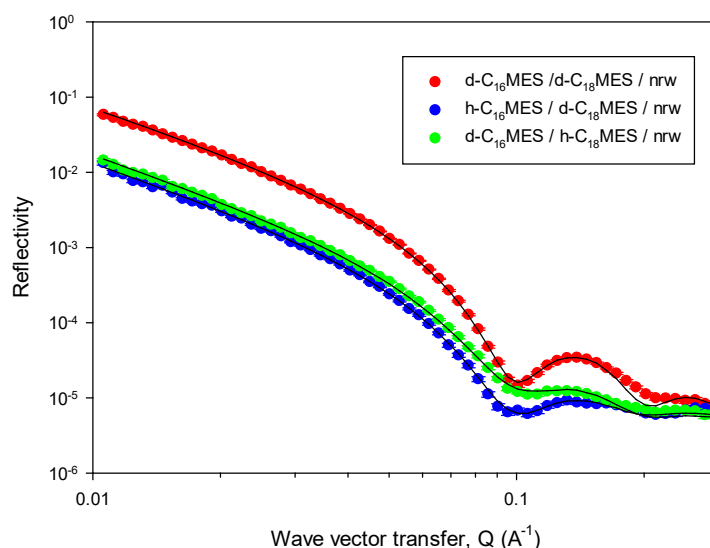


Figure 5. Neutron reflectivity data for 0.25 mM 65/35 mole ratio C_{16} -MES / C_{18} -MES mixture in 0.3 mM $AlCl_3$, see legend for details. The solid lines are model calculations as described in the text and for the key model parameters summarised in table 4.

In analysing the 4 different reflectivity profiles the model was constrained such that the thicknesses were held the same and only the scattering length densities of the different layers were allowed to vary. The key model parameters are summarised in table 4; and the mean thicknesses of each layer were 20.0, 6.0 and 33 ± 1 Å respectively; and broadly similar to those for the data and model in figure 3. The d.p values in the model for the isotopic combinations, d- C_{16} MES / d- C_{18} MES, and h- C_{16} MES / d- C_{18} MES were used to estimate the composition of the initial monolayer and the bilayer beneath. For the monolayer the composition was 0.54 mole fraction C_{16} -MES, and for the bilayer 0.53. This compares with the composition of the mixed monolayer in the absence of $AlCl_3$ ~ 0.53 mole fraction C_{16} -MES at a roughly equivalent point above the cmc.

(iv) Self-assembly of the C_{16} -MES / C_{18} -MES mixtures

The self-assembly and composition of the C_{16} -MES / C_{18} -MES eutectic mixture has been studied using SANS at relatively low surfactant concentrations, in the concentration range 5 to 20 mM. The measurements were made for the 65/35 mole ratio eutectic mixture of C_{16} -MES / C_{18} -MES in the absence of electrolyte and for the isotopic combinations d- C_{16} MES / h-

C₁₈MES, h-C₁₆MES / d-C₁₈MES and h-C₁₆MES / h-C₁₈MES in D₂O at surfactant concentrations of 5, 10 and 20 mM. The scattering data for 20 mM surfactant concentration are shown in figure 6. The data are consistent with globular interacting micelles, as discussed in detail later.

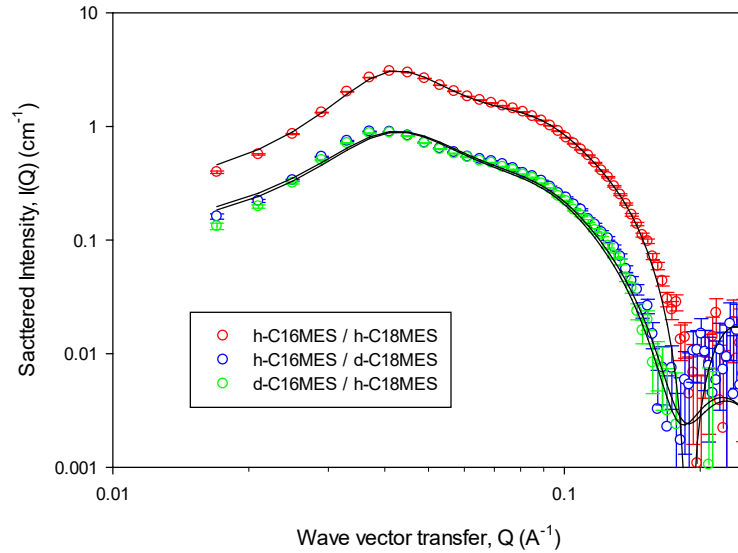


Figure 6. SANS data for 20 mM 65/35 mole ratio C₁₆-MES / C₁₈-MES in D₂O, and isotopic combinations d-C₁₆MES / h-C₁₈MES, h-C₁₆MES / d-C₁₈MES and h-C₁₆MES / h-C₁₈MES (see legend for details). The solid lines are model calculations as described in the text and for the key model parameters in table 6.

It was shown by Penfold et al (51) that the micelle compositions can be reliably calculated from the ratio of scattered intensities measured for different surfactant isotopic combinations. Assuming that $F(Q)$ and $S(Q)$ are ~ 1.0 at low Q or do not alter with isotopic content, then following Penfold et al (53),

$$I(Q) \approx NV^2(\rho_m - \rho_s)^2 \quad (5)$$

and from the ratio of the intensities, $R = I_{hh}/I_{hd}$ the volume fraction and mole fraction of the micelle can be obtained. As such from the hh, hd data for C₁₆ / C₁₈-MES the volume fraction, V_f , of C₁₈-MES is given as,

$$V_f = \frac{(\sqrt{R} - 1)(\rho_{h-C16} - \rho_{d2O})}{(\rho_{h-C18} - \rho_{h-C16}) - \sqrt{R}(\rho_{d-C18} - \rho_{h-C16})} \quad (6)$$

and the mole fraction, M_f , by

$$M_f = \frac{V_f / Vol_{C18}}{V_f / Vol_{C18} - (1 - V_f) / Vol_{C16}} \quad (7)$$

This then gives, taking V_{C18} , V_{C16} as 560, 511 Å³ respectively, and ρ_{d2o} , ρ_{h-C16} , ρ_{h-C18} , and ρ_{d-C18} as 6.35 x10⁻⁶, 6.1x10⁻⁷, 4.2 x10⁻⁷, and 6.56 x10⁻⁶ respectively, the parameters in the table 5 below.

Table 5. R , V_f , M_f values for C_{16} -MES / C_{18} -MES mixture

Concentration (mM)	R (hh/hd)	V_f (C ₁₈ -MES) ±0.05	M_f (C ₁₈ -MES) ±0.05
5	3.20	0.42	0.40
10	3.10	0.41	0.40
20	3.30	0.43	0.41

Notably in this concentration range the micelles are systematically richer in the more surface active C₁₈-MES; but closer (and within the error of the measurements) to the solution composition than the surface (see figure 4b). A detailed evaluation of the micelle composition and its variation with concentration using the pseudo phase approximation will be presented later in the discussion along with the surface mixing.

The SANS data for the 65/35 mole ratio C₁₆-MES / C₁₈-MES mixture are analysed using the core-shell model of interacting globular micelles developed by Hayter and Penfold (45). The core-shell model comprises of an inner core, radius R₁, containing alkyl chains packed in a space filling liquid alkane density, and an outer shell, radius R₂, determined by space filling and containing the headgroups and associated hydration. The inner core is constrained to a maximum dimension, l_c , the fully extended alkyl chain length. For an aggregation number, ν , which defines an inner volume larger than that defined by l_c , the shape becomes elliptical (prolate ellipse) with an elliptical ratio of ee . The inter-micellar interactions are accounted for by the RMSA screened coulombic potential which is defined by the hardsphere diameter, σ , ($\sigma=2R_2$), the surface charge, z , and the Debye-Hückel inverse screening length, κ , determined in the usual way by the ionic strength arising from the monomers, macroions (micelles) and any added electrolyte. Using known molecular volumes and neutron scattering lengths the form factor and structure factor can be calculated. The key refinable model

parameters are then the micelle aggregation number, v , and the micelle surface charge, z . Acceptable model fits require that the shape of the scattering is reproduced and the absolute value of the scattered intensity is predicted to within $\pm 20\%$; that is, the scale factor, sf , can vary in the range ~ 0.8 to 1.2 .

The data for the three different contrasts measured are analysed separately, but with the constraint that the micelle compositions, derived in table 5 using equations 5-7, are used. The key model parameters are summarised in full in table 6.

Table 6. Key model parameters for fits to SANS data in figure 7 for 65/35 mole ratio C_{16} -MES / C_{18} -MES in D_2O .

(a) 20 mM

Contrast combination	v (± 5)	z (± 2)	R1 (± 0.5)	R2 (± 0.5)	ext (± 0.05)	ee (± 0.02)	Sf
hh/ D_2O	122	34	22.7	27.1	1.2	1.0	0.95
hd/ D_2O	128	29	21.9	26.2	1.1	1.04	0.86
dh/ D_2O	125	29	22.5	27.0	1.1	1.04	0.62

(b) 10 mM

Contrast combination	v (± 5)	z (± 2)	R1 (± 0.5)	R2 (± 0.5)	ext (± 0.05)	ee (± 0.02)	Sf
hh/ D_2O	119	45	22.5	26.9	1.11	1.0	0.95
hd/ D_2O	117	37	22.3	26.7	1.12	1.0	0.76
dh/ D_2O	104	33	21.3	25.5	1.05	1.03	0.73

(c) 5 mM

Contrast combination	v (± 5)	z (± 2)	R1 (± 0.5)	R2 (± 0.5)	ext (± 0.05)	ee (± 0.02)	Sf
hh/ D_2O	110	58	21.8	26.1	1.09	1.0	0.91
hd/ D_2O	112	61	22.0	26.4	1.10	1.0	0.85
dh/ D_2O	112	55	22.0	26.2	1.10	1.0	0.65

The model parameters v , z , RI , $R2$, ee , ext , and sf are defined in the main text.

The mean values for v , δ and ee at 20, 10 and 5 mM are 123, 113, 115 \pm 5, 0.25, 0.35, 0.5 \pm 0.02, and 1.05, 1.01, 1.00 \pm 0.01 respectively. Due to the larger value for lc (19.7 and 21.7 Å for C_{16} and C_{18} alkyl chain lengths, compared to 16.7 Å for dodecyl alkyl chains such as in SDS and SLES), and an additional model parameter, ext , the C_{16} -MES / C_{18} -MES mixed micelles remain almost spherical ($ee \sim 1.0$), even though the aggregation number is > 100 . The parameter ext allows for the packing constraints of the inner core described earlier to be relaxed (29, 39, 52), enabling the inner core dimension to vary from lc to $lc \cdot ext$. For the C_{16} / C_{18} -MES mixtures ext varies from 1.05 to 1.2. The aggregation number is roughly constant over the concentration range explored, increasing only slightly as the concentration increases from 5 to 20 mM. Although still globular the micelles have a larger aggregation number by comparison with other broadly similar anionic surfactants, SDS and SLES, due to the increased alkyl chain length. The degree of ionisation, δ , is ~ 0.25 at the higher concentration of 20 mM, similar to that for SDS (45, 52), but notably larger than was observed for SLES (53). It increases significantly as the concentration decreases towards the cmc, and at 5 mM δ is ~ 0.5 . In general δ is observed to increase as the surfactant concentration decreases, as reported for SDS and a range of cationic surfactants (45, 52).

DISCUSSION

The adsorption isotherms for C_{16} -MES and C_{18} -MES are compared with that previously reported for C_{14} -MES (27) in figure 2. The two key features of the isotherms and their comparison with the isotherm for C_{14} -MES are their high degree of overlap when scaled to their respective cmc values and the lack of slope in the isotherm above the cmc.

As described earlier this overlap of the scaled isotherms and the invariance in the saturation adsorption values with alkyl chain length has been observed in other homologous series of anionic surfactants, notably the SLES surfactant with alkyl chain variations from 10 to 16 (32) and for the alkyl sulfates with alkyl chain variations from 8 to 14 (47). This is interpreted as implying that the saturated adsorption or limiting area / molecule is determined by the alkyl chain packing and the headgroup plays a more secondary role. This is not always the case and for the alkyl trimethyl ammonium cationic surfactants this is only the case when the alkyl chain length reaches a critical length (42).

The lack of slope in the isotherms above the cmc was also reported for the SLES surfactants (31, 32) where a detailed comparison with SDS in the presence and absence of electrolyte was

made (54). For SDS the adsorption continues to increase significantly above the cmc and it was demonstrated (54) that this was associated with a change in the mean activity due to a change in the degree of dissociation of the micellar phase. In contrast SLES, which has an almost constant adsorption above the cmc, has a much lower degree of dissociation and a relatively small change in the mean activity as the cmc increases above the cmc (54). The impact of NaCl on the saturation adsorption for C₁₄-MES, SLES and SDS was discussed by Xu et al (27, 28), and smaller increases in the saturation adsorption are observed for SLES and C₁₄-MES compared to SDS. This and the invariance in the adsorption above the cmc was attributed to the lower level of dissociation at the surface for SLES; and implies also a similar lower degree of dissociation for C₁₄-MES, C₁₆-MES and C₁₈-MES. The C₁₆-MES and C₁₈-MES solution structures were not measured separately, however analysis of the SANS data for the C₁₆ / C₁₈-MES mixture gives δ values similar to SDS. The similarity between the MES and SDS micelle degrees of ionisation implies that for these MES surfactants the degree of counterion dissociation is different at the surface and in the micellar phase; and reflects the more complex headgroup structure of the MES surfactant compared to SDS and SLES.

The impact of AlCl₃ on the surface adsorption properties of C₁₄-MES was extensively studied and reported by Xu et al (28). With increasing AlCl₃ concentration the surface adsorption evolved from a monolayer to surface multilayer formation with discrete numbers of bilayers, n , from 1 to 3, to eventually multilayer structures with large values of n , ≥ 20 , at higher AlCl₃ concentrations. It was shown that the evolution in the surface structure depended upon the surfactant and counterion concentrations. The structural evolution and associated surface phase diagram for C₁₄-MES exhibited all the features previously illustrated for SLES (31, 32) but showed how further manipulating the headgroup structure can impact upon the detailed pattern of the surface structure evolution. Xu et al (32) showed the impact of increasing the alkyl chain length and hence the solubility of the SLES surfactant on the surface structure in the presence of AlCl₃; and the closer proximity of the solubility limit and precipitation has a significant impact. Compared to the C₁₀ and C₁₂ alkyl chain length SLES surfactants the C₁₄ and C₁₆ chain length SLES surfactants exhibit a narrower region of multilayer formation, with a decrease in the surface ordering at higher AlCl₃ concentrations due to precipitation such that for the C₁₆ chain length the surface eventually reverts to a monolayer. This results from the surface now being in equilibrium with a more dilute solution phase. For the C₁₆ and C₁₈-MES the closer proximity of precipitation in the presence of AlCl₃ has a broadly similar impact to the longer alkyl chain length SLES surfactants; but in detail there are some notable differences. For C₁₆-

MES at a surfactant concentration of 0.8 mM and for AlCl_3 concentrations from 0.1 to 0.5 mM the surface structure changes from a monolayer in the absence of AlCl_3 and at 0.005mM AlCl_3 to a three layer structure, corresponding to an initial monolayer and a single bilayer beneath, which does not change over that AlCl_3 concentration range. For C_{14} -MES (28) and SLES (31, 32), at a similar surfactant concentration and AlCl_3 concentration range a more extensive evolution in the surface structure, extended multilayer structures and a region with discrete small numbers of bilayers, are observed. For C_{18} -MES at a surfactant concentration of 0.2 mM and over the same AlCl_3 concentration range the reflectivity is dominated entirely by the impact of precipitation in the bulk solution. Hence for C_{16} -MES the absence of the more extended surface structures and the occurrence of only a three layer structure, and the onset of precipitation for C_{18} -MES before any surface ordering occurs contrasts strongly with the observations for C_{14} -MES (28) and SLES (31, 32). This implies that for the addition of AlCl_3 as the alkyl chain length increases the onset of precipitation occurs more readily for the MES than for the SLES surfactants. This is attributed to the headgroup structure that must disfavour the binding of the Al^{3+} ions within the surface plane and the bridging across layers which results in the attractive force which drives the surface multilayer formation in SLES. This provides an important insight into how the nature of the headgroup geometry affects the counterion binding and the evolution in the surface structure.

The surfactant mixing for the $\text{C}_{16} / \text{C}_{18}$ -MES mixture at a fixed solution composition of 65/35 mole ratio $\text{C}_{16} / \text{C}_{18}$ -MES, the eutectic mixture, has been measured at the air-water interface using NR over the concentration range of 0.1 to 10 mM, from below to well above the mixed cmc, see figure 4. The micelle composition for the same solution composition has been measured by SANS in the concentration range of 5 to 20 mM, see tables 5 and 6 and figure 7.

Table 7. *Pseudo phase approximation model parameters for C_{16} -MES / C_{18} -MES micelle and surface mixtures.*

C_{16} -MES: Area/molecule at cmc=50 Å², Cmc=0.73 mM, Surface tension at cmc=37 mN/m

C_{18} -MES: Area/molecule at cmc=52 Å², Cmc=0.25 mM, Surface tension at cmc=38 mN/m

$$\beta_{\text{micelle}} = 1.4, \beta_{\text{surface}} = 1.5$$

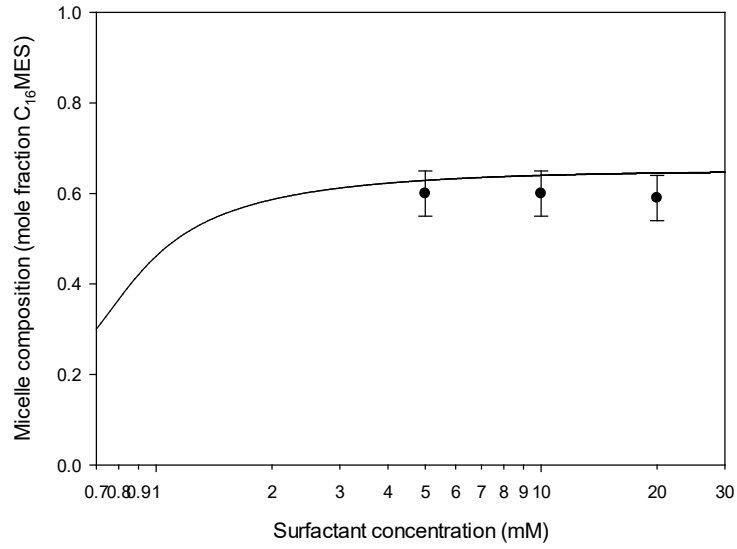


Figure 7. Variation in micelle composition with surfactant concentration for 65/35 mole ratio $C_{16}-MES / C_{18}-MES$. The solid line is the calculated variation from the pseudo phase approximation for the parameters summarised in table 7.

In order to more fully understand the mixing properties at the surface and in micelles the data can be interpreted by two limiting approaches, a rigorous or approximate thermodynamic approach such as the pseudo phase approximation (55, 56) or using statistical mechanics, such as the molecular thermodynamic approach (57, 58). Here the surface and micelle compositions have been calculated using the pseudo phase approximation in which quadratic and cubic terms are included in the description of the excess free energy of mixing. Recent studies (59-61) have shown this approach to be particularly powerful in describing complex surfactant mixtures.

In the pseudo phase approximation, at equilibrium the chemical potential of the components of the pseudo phase, micelles, surface and solution monomer, are equal (55, 56); and equating the chemical potential of the micelle and monomer, for example, gives,

$$x_i = \frac{c_i^{mon}}{f_i^m c_i^\mu} \quad (8)$$

where x_i is the mole fraction of the i^{th} component in the micelle, c_i^{mon} the monomer concentration of the i^{th} component, f_i^μ its activity coefficient in the micelle, and c_i^μ its cmc. For a binary mixture, assuming the micelle mole fractions equal unity and at the cmc $c_i^{mon} = \alpha_i c_i^{mix}$, where α_i is the mole fraction of monomer in solution and c_{mix}^μ the mixed cmc,

$$\frac{1}{c_{mix}^{\mu}} = \frac{\alpha_1}{f_1 c_1^{\mu}} + \frac{\alpha_2}{f_2 c_2^{\mu}} \quad (9)$$

The activity coefficients are derived from an expansion of the excess free energy of mixing, G_e , which includes quadratic and cubic terms in the form,

$$G_e = x_1 x_2 \beta_{12} + x_1 x_2 (x_1 - x_2) C_{12} \quad (10)$$

where β_{12} and C_{12} are the interaction constants. In the Regular Solution Approximation C_{12} is zero. As described in detail elsewhere (59-61) this leads to a set of equations that can be solved iteratively to obtain the cmc variation, the variations in micelle compositions and the variation in surface and monomer concentrations below and above the cmc. In the application of the PPS to the surface and micelle data presented here the same model parameters are constrained to model both data, and this provides a strong constraint on the parameters.

In figure 4b the solid and dashed lines are the calculated variation in the surface composition using the PPA as described above. The key model parameters for the PPA calculations are summarised in table 7. Using the known cmc and surface tension values the data are within error well described using only the quadratic terms, β_{12} , in the expansion of the excess free energy of mixing. The analysis shows that at the surface, $\beta_s=1.5$, and in the micelles, $\beta_m=1.4$, with both cubic coefficients zero; that is, the interaction between the two surfactants is repulsive. The PPA analysis of the surface data provides a good description of the evolution in the surface composition with concentration, from below the cmc to concentrations well in excess of the cmc. The impact of the onset of micellisation on the surface composition is evident and the surface composition changes markedly at the cmc. Below the cmc the surface is in equilibrium with monomers in solution, whereas above the cmc the equilibrium changes and the surface and monomers are now in equilibrium with the micellar phase.

The corresponding variation in the micellar composition is shown in figure 7, and within experimental error the data and calculations are in good agreement. The variation in the micellar composition with concentration, over the limited concentration range explored, is less marked. However the values show the expected trend, that as the solution concentration increases the micelle composition tends towards the solution composition.

Although over the concentration range measured the surface and micelle compositions are different to the solution composition, they are within the PPA predictions, and the micelle composition shows the expected trend towards the solution composition as the surfactant

concentration increases. The surface and micelles have different compositions is not unusual or unexpected. Whereas the micelle composition must tend towards the solution composition in the limit of high concentrations, the surface does not have that constraint. The surface and monomer components can adopt a different composition as seen here, and as illustrated previously in non-ionic surfactant mixtures (50) and in non-ionic / anionic surfactant mixtures (51).

The observation of a repulsive interaction, positive interaction parameter, close to phase separation has important implications for the interpretation of eutectic surfactant mixtures. Moroi et al (36) investigated the phase equilibrium in mixtures of anionic surfactants, SDS with different divalent metal dodecyl sulfates, and the phase diagrams and Krafft point minima determined were ascribed to a eutectic point. Tsujii et al (37) investigated the Krafft point variations in the sodium and calcium salts of a range of different anionic surfactants, and in most cases a Krafft point minimum was obtained and interpreted in terms of eutectic mixtures. Scamehorn et al (38, 39) made similar observations on the behaviour of mixtures of anionic surfactants with different chain lengths and isomeric forms. Tsujii et al (37) interpreted the Krafft point as the melting temperature of the hydrated solid surfactant and hence the observed immiscibility was consistent with freezing point depression of the associated solid phases of the different components. Hence the Krafft point minimum was attributed to a eutectic point, and the usual thermodynamical treatment of freezing point depression was able to predict the Krafft point variation with composition. For two solids to form a simple eutectic requires that the pure solids are stable solid phases and a mixed solid phase does not form, and hence the immiscibility reported by Tsujii et al. The eutectic is then the result of each solid dissolving to form a dilute solution in the other as the liquid solvent. Since the solid phases are immiscible in a simple eutectic this implies a repulsive interaction between the two surfactants. The C₁₆- / C₁₈-MES mixture exhibits a Krafft point minimum (35). Furthermore we have demonstrated here that the surface and micelle mixing are consistent with a repulsive interaction, positive interaction parameter, which is close to phase separation. For example a positive interaction parameter of ≥ 2.0 in the regular solution approximation results in phase separation. Hence the assumption made by Moroi et al (36), Tsujii et al (37) and Scamehorn et al (38, 39) that the behaviour of mixtures like the C₁₆- / C₁₈-MES mixture is analogous with eutectic behaviour seems well justified.

CONCLUSIONS

The NR and SANS measurements have extended greatly our understanding of the adsorption and self-assembly of the MES surfactant, and will provide the key information required for their wider exploitation as sustainable surfactants (13-26). The comparison of the adsorption isotherms of C₁₄ to C₁₈-MES, their scaling with their cmc values, and the invariance in the saturation adsorption reinforces the conclusions from previous studies on other anionic surfactants (32, 47) that the saturation adsorption or limiting area / molecule is determined by the alkyl chain packing and that the headgroup plays a more secondary role. The structure of the MES surfactant, which confers some tolerance to hardwater conditions (18-22), results in the inhibition of precipitation to a sufficient degree for the addition of multivalent counterions to induce surface multilayer formation and micellar growth. This is broadly similar to that observed for SLES (29, 30, 53), and also extends earlier measurements on C₁₄-MES (28). However, for the longer alkyl chain length surfactants, C₁₆, C₁₈-MES, the closer proximity of the precipitation boundary limits the range of surface structures observed and for C₁₄ to C₁₈-MES results in only nominal micellar growth before precipitation occurs. The Krafft point minimum reported for C₁₆ / C₁₈-MES mixtures (35) extends significantly the potential application of the longer alkyl chain surfactants. The variation in the surface and micelle compositions determined here are well described by the pseudo phase approximation with repulsive interactions, positive interaction parameter, with values relatively close to those for phase separation. The repulsive interaction supports the analogy with eutectic mixtures (36-39) and explain the mixing properties of these and related surfactant mixtures.

ACKNOWLEDGEMENTS

The provision of beam time on the INTER reflectometer and the LOQ diffractometer at ISIS is acknowledged. The invaluable scientific and technical input and support from the staff at ISIS is greatly appreciated.

SUPPORTING INFORMATION

Additional tables are included in the Supporting Information

REFERENCES

- (1) J. J. Scheibel, The evolution of anionic surfactant technology to meet the requirements of the laundry detergent industry, *J. Surf. Det.* 2004, 7, 319-328
- (2) Y U Yangxin, Z Jin, A E Bayley, Development of surfactants and builders in detergent formulations, *Chinese J. Chem. Eng.* 2008, 16, 517-527
- (3) J F Scamehorn in "Phenomena in mixed surfactant systems", Ed J F Scamehorn, ACS Symp. Ser. 311, ACS Washington DC, 1988
- (4) M J Rosen in "Phenomena in mixed surfactant systems", Ed J F Scamehorn, ACS Symp. Ser. 311, ACS Washington DC, 1988
- (5) K L Steller, J F Scamehorn, Surfactant precipitation in aqueous solutions containing mixtures of anionic and non-ionic surfactants, *J. Am. Oil Chem. Soc.* 1986, 63, 566-574
- (6) P Paton-Morales, F I Talens-Alessen, Effect of ionic strength and competitive adsorption of Na^+ on the flocculation of Lauryl sulfate micelles with Al^{3+} , *Langmuir*, 2001, 17, 6059-6064
- (7) B L Chou, J H Bae, Surfactant precipitation and redissolution in brine, *J. Coll. Int. Sci.* 1983, 96, 192-203
- (8) A Sein, J B F N Engberts, E van der Linden, J van der Pas, Lyotropic phase of dodecyl benzene sulfonates with different counterions in water, *Langmuir*, 1996, 12, 2913-2923
- (9) R G Alargova, K D Danov, P A Kralchevsky, G Broze, A Mahreteab, Growth of giant rodlike micelles in ionic surfactants in the presence of Al^{3+} counterions, *Langmuir*, 1998, 14, 4036-4049
- (10) R G Alargova, V P Ivanova, P A Kralchevsky, A Mahreteab, G Broze, Growth of rodlike micelles in anionic surfactant solutions in the presence of Ca^{2+} counterions, *Coll. Surf. A* 1998, 142, 201-218
- (11) J H Mu, G Z Li, Rheology of viscoelastic anionic micellar solutions in the presence of multivalent counterions, *Coll. Polym. Sci.* 2001, 279, 872-875
- (12) I Johansson, M Svensson, Surfactants based on fatty acids and other natural hydrophobes, *Curr. Opin. Coll. Int. Sci.* 2001, 6, 178-188
- (13) Z A Maurad, R Ghazali, P Siwayanan, Z Ismail, S Ahmad, α -sulfonated methyl esters as an active ingredient in palm-based powder detergents, *J. Surf. Det.* 2006, 9, 161-167

- (14) D Martinez, G Orozoco, S Rincon, I Gil, Simulation and pre-feasibility analysis of the production process of α -methyl ester sulfonates, *Bioresource Technol.* 2010, 101, 8762-8771
- (15) S Ahmad, P Siwayanan, H A Murad, H A Aziz, H Seng Soi, Beyond biodiesel, methyl esters as a route for the production of surfactant feedstocks, *Inform*, 2007, 18, 216-228
- (16) L Cohen, F Soto, M S Imura, Separation and extraction of ϕ methyl ester sulfonates: new features, *J. Surf. Det.* 2001, 4, 73-74
- (17) W Stein, H Haumann, α -sulfonated fatty acids and esters: manufacturing, process, properties and applications, *JAACS*, 1975, 52, 323-329
- (18) J Aparicio, B W MacArthur, W B Sheats, B J Brooks, MES-myths, mysteries and perspective on properties and use, *ICSD*, 2012, Shanghai, PRC
- (19) D W Roberts, Aquatic toxicity – are surfactant properties relevant, *J. Surf. Det.* 2000, 3, 309-315
- (20) R Ghazali, Z A Maurad, P Siwayanan, M Yusof, A Ahmad, Assessment of aquatic effects on palm-based α -sulfonated methyl esters, *J. Oil Palm Res.* 2006, 18, 225-230
- (21) R Ghazali, A Ahmad, Biodegradability and ecotoxicity of palm stearin based methyl ester sulfonates, *J. Oil Palm Res.* 2004, 16, 39-44
- (22) R Ghazali, The effect of disalt on the biodegradability of methyl ester sulfonates, MES, *J. Oil Palm Res.* 2002, 14, 45-50
- (23) L Cohen, F Trujillo, Synthesis, characterisation and surface properties of sulfonated methyl esters, *J. Surf. Det.* 1998, 1, 338-341
- (24) K Ohbu, M Fujiwara, Y Abu, Physicochemical properties of α -sulfonated fatty acid esters, *Prog. Coll. Polym. Sci.* 1998, 109, 85-92
- (25) S P Wong, W H Lim, S F Cheng, C H Chuah, Properties of sodium methyl ester 4-sulfoalkylate / trimethyl ammonium bromide mixtures, *J. Surf. Det.* 2012, 15, 601-611
- (26) K D Danov, R D Stanimirova, P A Kralchevsky, E S Basheva, V I Ivanova, J T Petkov, Sulfonated methyl esters of fatty acids in aqueous solution: interfacial and micellar properties, *J. Coll. Int. Sci.* 2015, 457, 307-318
- (27) H Xu, P X Li, K Ma, R Welbourn, J Penfold, D W Roberts, R K Thomas, J T Petkov, Adsorption of methyl ester sulfonate at the air-water interface: can limitations

- in the application of the Gibbs equation be overcome by ‘computer purification’,
Langmuir, 2017, 33, 9944-9953
- (28) H Xu, R K Thomas, J Penfold, P X li, K Ma, R Welbourn, D W Roberts, J T Petkov, The impact of electrolyte on the adsorption of the anionic surfactant methyl ester sulfonate at the air-solution interface: surface multilayer formation, J. Coll. Int. Sci. 2017, 512, 231-238
 - (29) J Penfold, R K Thomas, C C Dong, I Tucker, K Metcalfe, S Golding, I Grillo, Equilibrium surface adsorption behaviour in complex anionic / non-ionic surfactant mixtures, Langmuir, 2007, 23, 10140-10149
 - (30) J T Petkov, I M Tucker, J Penfold, R K Thomas, D N Petsev, C C Dong, S Golding, I Grillo, The impact of multivalent counterions Al^{3+} on the surface adsorption and self-assembly of the anionic alkyloxyethylene sulfate and anionic / non-ionic surfactant mixtures, Langmuir, 2010, 26, 16691-16709
 - (31) H Xu, J Penfold, R K Thomas, J T Petkov, I Tucker, J R P Webster, The formation of surface multilayers at the air-water interface from sodium polyethylene glycol monoalkyl ether sulfate / $AlCl_3$ solutions: the role of the size of the polyethylene oxide group, Langmuir, 2013, 29, 11656-11666
 - (32) H Xu, J Penfold, R K Thomas, J T Petkov, I Tucker, J R P Webster, The formation of surface multilayers at the air-water interface from sodium polyethylene glycol monoalkyl ether sulfate / $AlCl_3$ solutions: the role of the alkyl chain length, Langmuir, 2013, 29, 12744-12753
 - (33) R Bradbury, J Penfold, R K Thomas, I M Tucker, J T Petkov, C Jones, Enhanced perfume delivery to interfaces using surface multilayer structures, J. Coll.Int. Sci. 2016, 463, 199-206
 - (34) T Satsuki, Applications of MES in detergents, Inform, 1992, 3(10), 1099
 - (35) F Schambil, M J Schwuger, Physical-chemical properties of α -sulfo fatty acid methyl esters and α -sulfo fatty acid disalts, Tenside, 1990, 27, 380-385
 - (36) Y Moroi, T Oyama, R Matuura, Phase equilibria of anionic surfactant mixtures in aqueous solution, J. Coll. Int. Sci. 1977, 60, 103-111
 - (37) K Tsujil, N Salto, T Takesuchi, Krafft points of anionic surfactants and their mixtures with the special attention to their applicability in hard water, J. Phys. Chem. 1980, 84, 2287-2291

- (38) J F Scamehorn, J H Harwell, Precipitation in surfactant mixtures, Chapt 10, page 203, in Mixed Surfactant systems, Eds K Ogino, M Abe, Surfactant Science Series, Vol 46, Marcel Dekker, NY, 1992
- (39) J F Scamehorn, J H Harwell, Chapt 18, page 601, Mixed Surfactant Systems, Surfactant Science Series, Eds M Abe, J F Scamehorn, Marcel Dekker, NY, 2005
- (40) H Fauzi, H S C Metselaar, T M I Mahlia, M Silakhori, Phase change material: optimising the thermal properties and thermal conductivity of myristic acid / palmitic acid eutectic mixtures with acid based surfactants, Appl. Thermal Eng. 2013, 60, 261-265
- (41) INTER reflectometer at the ISIS Facility, <http://www.isis.stfc.ac.uk/instruments/INTER>
- (42) J R Lu, R K Thomas, J Penfold, Surfactant layers at the air-water interface: structure and composition, Adv. Coll. Int. Sci. 2000, 84, 143-304
- (43) LOQ diffractometer at the ISIS facility, <http://www.isis.stfc.ac.uk/instruments/LOQ>
- (44) R K Heenan, S M King, R Osborn, H B Stanley, RAL Internal report, RAL-89-128, 1989
- (45) J B Hayter, J Penfold, Determination of micelle structure and charge by SANS, Coll. Polym. Sci. 1983, 26, 1022-1030
- (46) J B Hayter, J Penfold, An analytic structure factor for macrion solutions, Mol. Phys. 1981, 42, 109-118
- (47) I Varga, R Meszaros, T Gilanyi, Adsorption of sodium alkyl sulfate homologues at the air/solution interface, J. Phys. Chem. B, 2007, 111, 7160-7168
- (48) MB11a subroutine in the Harwell Subroutine Library. www.hs1.rl.ac.uk
- (49) J H Clint, Micellisation in mixed non-ionic surface active agents, J. Chem. Soc. Faraday Trans. I, 1975, 71, 1327-1334
- (50) J Penfold, E Staples, L Thompson, I Tucker, The composition of non-ionic surfactant mixtures at the air-water interface as determined by neutron reflectivity, Coll. Surf. 1995, 102, 107-132
- (51) J Penfold, R K Thomas, J R Lu, Solution and adsorption behaviour of the mixed surfactant system SDS / C₁₂E₆, Langmuir, 1995, 11, 2496-2508

- (52) J B Hayter, A self-consistent theory of dressed micelles, *Langmuir*, 1992, 8, 2873-2876
- (53) H Xu, J Penfold, R K Thomas, J T Petkov, I Tucker, A Terry, The impact of AlCl_3 on the self-assembly of the anionic surfactant sodium oligoethylene glycol monoalkyl ether sulfate in aqueous solution, *Langmuir*, 2013, 29, 13359-13366
- (54) H Xu, P X Li, K Ma, R K Thomas, J Penfold, J R Lu, Limitations in the application of the Gibbs equation to anionic surfactants at the air-water interface: sodium dodecylsulfate and sodium dodecylmonooxyethylenesulfate above and below the cmc, *Langmuir*, 2013, 29, 9335-9351
- (55) P M Holland, Non-ideal mixed micelle solutions, *Adv. Coll. Int. Sci.* 1986, 26, 111-129
- (56) P M Holland, D N Rubingh, Non-ideal multicomponent mixed micelle model, *J. Phys. Chem.* 1983, 87, 1984-1990
- (57) R Nagarajan, E Ruckenstein, Theory of surfactant self-assembly, a predictive molecular thermodynamic approach, *Langmuir*, 1991, 7, 2934-2969
- (58) A Shiloach, D Blankschtein, Predicting micellar solution properties in binary surfactant mixtures, *Langmuir*, 1998, 14, 1618-1638
- (59) P X Li, K Ma, R K Thomas, J Penfold, Analysis of the asymmetrical synergy in the adsorption of zwitterionic-ionic surfactant mixtures at the air-water interface below and above the cmc, *J. Phys. Chem. B*, 2016, 120, 3677-3691
- (60) J Liley, R K Thomas, J Penfold, I M Tucker, J T Petkov, P Stevenson, J R P Webster, Surfactant adsorption in ternary surfactant mixtures above the cmc; the importance of the shape of the excess free energy, *J Phys. Chem. B*, 2017, 121, 2825-2838
- (61) J Liley, R K Thomas, J Penfold, I M Tucker, J T Petkov, P Stevenson, J R P Webster, The impact of electrolyte on the adsorption at the air-water interface for a ternary surfactant mixture above the cmc, *Langmuir*, 2017, 33, 4301-4312

SUPPORTING INFORMATION

TABLES

Table S1. Adsorption isotherm data for C_{16} , C_{18} -MES in figure 2 from NR data

(a) C_{16} -MES

Surfactant concentration (mM)	d (± 1 Å)	ρ ($\pm 0.05 \times 10^{-6}$ Å ⁻²)	A (± 2 Å ²)	Γ ($\pm 0.1 \times 10^{-10}$ mol cm ⁻²)
0.1	17	2.5	80	2.1
0.3	18	3.15	59	2.9
0.5	21	2.9	54	3.1
0.7	19	3.4	52	3.2
1.0	19	3.4	52	3.2
1.5	19	3.3	52	3.2
2.0	19	3.4	52	3.2

(b) C_{18} -MES

Surfactant concentration (mM)	d (± 1 Å)	ρ ($\pm 0.05 \times 10^{-6}$ Å ⁻²)	A (± 2 Å ²)	Γ ($\pm 0.1 \times 10^{-10}$ mol cm ⁻²)
0.1	19	3.0	64	2.6
0.2	20	3.65	51	3.3
0.3	20	3.8	50	3.3
0.5	19	4.0	50	3.3

d and ρ are the adsorbed monolayer thicknesses and scattering length density, A the area/molecule and Γ the adsorbed amount (as defined in equations 1 and 2 in the main text)